

Supporting Information

2D-Metal-organic coordination polymers of lanthanides (La(III), Pr(III) and Nd(III)) with redox-active dioxolene bridging ligand

Alexandr D. Kharitonov, Olesya Yu. Trofimova, Irina N. Meshcheryakova, Georgy K. Fukin, Mikhail N. Khrizanforov, Yulia H. Budnikova, Atem S. Bogomyakov, Rinat R. Aysin, Konstantin A. Kovalenko and Alexandr V. Piskunov

Table of Contents

Materials and methods.....	2
Experimental details.....	3
Table S1. Crystal data and structure refinement for 1-3	4
Table S2. Selected bond lengths (Å) for the compounds 1-3	5
Table S3. The parameters of porous structure of samples under investigation.....	6
Fig. S1. Pore size distribution curves for compounds 1 and 3	6
Fig. S2. CV of reduction for 1 . CPE, CH ₃ CN, 10 ⁻¹ M Bu ₄ NBF ₄ . Potentials vs. Ag/AgCl. Inset: Semi-Derivative of current vs potentials.....	7
Fig. S3. CV of oxidation for 1 . CPE, CH ₃ CN, 10 ⁻¹ M Bu ₄ NBF ₄ . Potentials vs. Ag/AgCl. Inset: Semi-Derivative of current vs potentials.....	7
Fig. S4. CV of reduction for 2 . CPE, CH ₃ CN, 10 ⁻¹ M Bu ₄ NBF ₄ . Potentials vs. Ag/AgCl. Inset: Semi-Derivative of current vs potentials.....	8
Fig. S5. CV of oxidation for 2 , CPE, CH ₃ CN, 10 ⁻¹ M Bu ₄ NBF ₄ . Potentials vs. Ag/AgCl. Inset: Semi-Derivative of current vs potentials.....	8
Fig. S6. CV of reduction for 3 . CPE, CH ₃ CN, 10 ⁻¹ M Bu ₄ NBF ₄ . Potentials vs. Ag/AgCl. Inset: Semi-Derivative of current vs potentials.....	9
Fig. S7. CV of oxidation for 3 , CPE, CH ₃ CN, 10 ⁻¹ M Bu ₄ NBF ₄ . Potentials vs. Ag/AgCl. Inset: Semi-Derivative of current vs potentials.....	9
Table S4. Frontier orbitals energy levels.....	9
Shape analysis.....	10
Fig S8. User-defined perfect polyhedron – one-capped Pentagonal Bipyramid.....	12
Fig. S9. PXRD patterns for 1 (blue line – experimental, red line – simulated).....	13
Fig. S10. PXRD patterns for 2 (blue line – experimental, red line – simulated).....	13
Fig. S11. PXRD patterns for 3 (blue line – experimental, red line – simulated).....	13
References.....	14

Materials and methods

All reactants were purchased from Sigma Aldrich. 2,5-dihydroxy-3,6-di-tert-butyl-p-benzoquinone was synthesized according to the previously reported procedure [1]. All synthetic manipulations were performed under Schlenk line conditions. Solvents were purified by standard methods [2]. Elemental analyses were performed with an Elementar Vario El cube instrument. Electronic absorption (UV-vis) spectra in range 200-900 nm of nujol mulls were recorded on a Carl Zeiss Jena Specord M400 spectrophotometer. IR-spectra of studied compounds were recorded on a FSM1201 Fourier-IR spectrometer in a nujol using KBr plates in the range 4000–400 cm^{-1} .

The magnetic susceptibility of the polycrystalline complexes was measured with a Quantum Design MPMSXL SQUID magnetometer in the temperature range 2–300 K with magnetic field of up to 5 kOe. None of complexes exhibited any field dependence of molar magnetization at low temperatures. Diamagnetic corrections were made using the Pascal constants. The effective magnetic moment was calculated as $\mu_{\text{eff}}(T) = [(3k/N_A\mu_B^2)\chi T]^{1/2} \approx (8\chi T)^{1/2}$.

The X-ray data for were collected on an Agilent Xcalibur E diffractometer (MoK_α -radiation, ω -scans technique, $\lambda = 0.71073 \text{ \AA}$, $T = 100 \text{ K}$) using and *CrysAlisPro* [3] software packages. The structures were solved by dual methods and were refined by full-matrix least squares on F^2 for all data using *SHELXTL* package [4]. Analytical numeric absorption correction using a multifaceted crystal model based on expressions derived by R.C. Clark & J.S. Reid [5] was used. All non-hydrogen atoms were found from Fourier syntheses of electron density and were refined anisotropically. Hydrogen atoms were placed in calculated positions and were refined in the “riding” model with $U(H)_{\text{iso}} = 1.2U_{\text{eq}}$ of their parent atoms ($U(H)_{\text{iso}} = 1.5U_{\text{eq}}$ for methyl groups). CCDC – 2005205 - 2005207 (**1-3**) contains the supplementary crystallographic data for this paper. These data are provided free of charge by The Cambridge Crystallographic Data Centre: ccdc.cam.ac.uk/structures. The crystallographic data and structure refinement details for **1 - 3** are given in ESI in Table S1.

An analysis of the porous structure was performed by a carbon dioxide adsorption technique using Quantochrome’s Autosorb iQ at 195 K. Cryostat CryoCooler was used to adjust temperature with 0.05 K accuracy. Carbon dioxide adsorption–desorption isotherms were measured within the range of relative pressures from 10^{-3} till 0.995. The specific surface area

was calculated from the data obtained on the basis of the conventional BET, Langmuir and DFT models. Pore size distributions were calculated using DFT method. The database of the National Institute of Standards and Technology [6] was used as a source of p–V–T relations at experimental pressures and temperatures.

Electrochemical measurements were performed on a BASiEpsilonE2P electrochemical analyzer (USA). The program handles wave Epsilon-EC-USB-V200. A conventional three-electrode system was used with glassy carbon for solutions or carbon paste electrode (CPE) for powder samples as the working electrode, the Ag/AgCl (0.01M) electrode as the reference electrode and a Pt wire as the counter electrode. 0.1 M Et₄NBF₄ was used as the supporting electrolyte for the determination of current—voltage characteristics. Acetonitrile was distilled over P₂O₅ and KMnO₄, and then over molecular sieves. After purification, the solvent was stored under dry argon. Used as a base salt, Et₄NBF₄ was recrystallized from ethanol and dried in a vacuum chamber at 100 °C for 2 days. To study powder samples, a modified CPE working electrode was used. Its preparation was as follows: the carbon particles/ phosphonium salt (dodecyl(tri-tert-butyl)phosphonium tetrafluoroborate) composite electrode was prepared by grinding a mixture of graphite powder and phosphonium salt in a ratio of 90/10 (w/w) in a mortar to give the homogeneous mass [7-10]. A modified electrode was made in a similar manner except that a part (ca. 5%) of graphite powder was replaced by the complex under investigation. A portion of the resulting paste was packed firmly into the cavity (3 mm in diameter) of a Teflon holder.

X-ray powder diffraction measurements were performed on Shimadzu LabX XRD-6100 X-ray Powder Diffractometer.

Experimental details.

Synthesis of 1. A mixture of solid LaCl₃·7H₂O (37 mg, 0.1 mmol) and H₂pQ (25 mg, 0.1 mmol) were placed in a glass ampoule and N,N'-dimethylacetamide (5 mL) was added. Ampoule was evacuated, sealed and heated at 130°C for 1 day. The obtained burgundy crystals were separated by the filtration, washed twice by 5 ml of N,N'-dimethylacetamide and dried on air.

Yield 0.34 mg (74 %). C₅₈H₉₀La₂N₄O₁₆. Calculated C, 50.58; H, 6.59; N 4.07 %. Found C, 50.72; H, 6.67; N 3.96 %. IR (Nujol, KBr) cm⁻¹: 1640(w), 1615(w), 1590(m), 1535(w), 1339(w), 1268(m), 1212(m), 1200(m), 1051(m), 1033(m), 1022(m), 969(m), 924(s), 900(m), 797(m), 744(m), 656(w), 624(s), 595(w), 480(w).

Synthesis of 2. Synthesis was performed according to the procedure for complex **1** with $\text{PrCl}_3 \cdot 6\text{H}_2\text{O}$ (36 mg, 0.1 mmol).

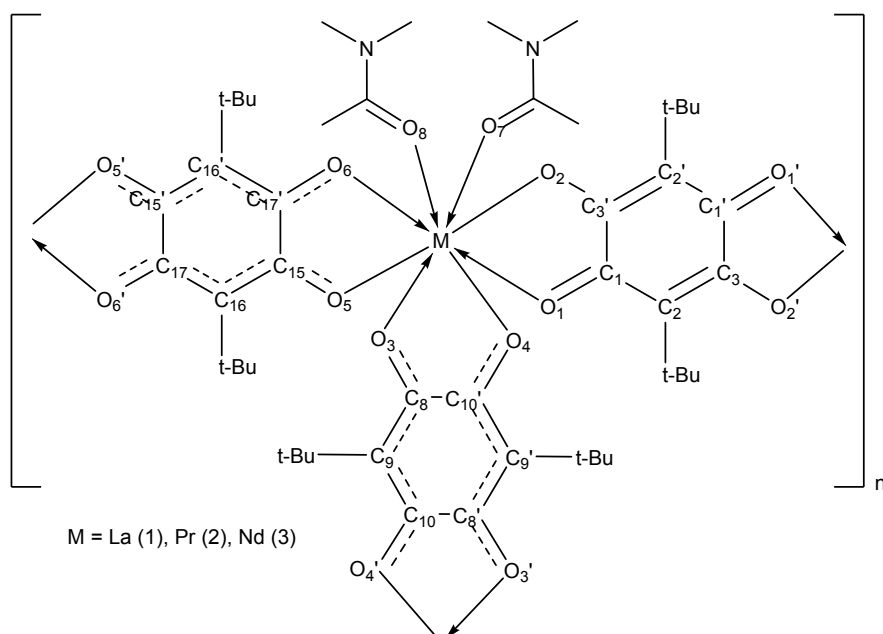
Yield 0.30 mg (65 %). $\text{C}_{58}\text{H}_{90}\text{Pr}_2\text{N}_4\text{O}_{16}$. Calculated C, 50.44; H, 6.57; N 4.06 %. Found C, 50.79; H, 6.65; N 3.94 %. IR (Nujol, KBr) cm^{-1} : 1639(w), 1613(w), 1591(m), 1538(w), 1338(w), 1265(m), 1212(m), 1198(m), 1050(m), 1034(m), 1021(m), 969(m), 922(s), 899(m), 794(m), 745(m), 657(w), 625(s), 596(w), 484(w).

Synthesis of 3. Synthesis was performed according to the procedure for complex **1** with $\text{NdCl}_3 \cdot 6\text{H}_2\text{O}$ (36 mg, 0.1 mmol).

Yield 0.37 mg (80 %). $\text{C}_{58}\text{H}_{90}\text{Nd}_2\text{N}_4\text{O}_{16}$. Calculated C, 50.19; H, 6.54; N 4.04 %. Found C, 50.51; H, 6.83; N 3.89 %. IR (Nujol, KBr) cm^{-1} : 1642(w), 1614(w), 1591(m), 1540(w), 1340(w), 1266(m), 1212(m), 1197(m), 1052(m), 1038(m), 1020(m), 970(m), 923(s), 900(m), 794(m), 753(m), 656(w), 623(s), 596(w), 486(w).

Table S1. Crystal data and structure refinement for **1-3**.

Compound	1	2	3
Formula	$\text{C}_{29}\text{H}_{45}\text{LaN}_2\text{O}_8$	$\text{C}_{29}\text{H}_{45}\text{PrN}_2\text{O}_8$	$\text{C}_{58}\text{H}_{90}\text{Nd}_2\text{N}_4\text{O}_{16}$
Formula weight	688.58	690.58	1387.81
Crystal system	Triclinic	Triclinic	Triclinic
Space group	P-1	P-1	P-1
a, Å	10.8245(4)	10.8462(4)	10.8521(3)
b, Å	12.1894(3)	12.2567(4)	12.2651(4)
c, Å	13.0365(4)	13.0356(4)	13.0496(4)
α , °	81.940(2)	80.342(3)	79.711(3)
β , °	69.924(3)	69.642(3)	69.400(3)
γ , °	84.811(2)	84.833(3)	84.672(3)
V, Å ³	1597.96(9)	1600.72(10)	1598.87(9)
Z	2	2	1
ρ , Mg/m ³	1.431	1.433	1.441
θ range, °	3.014 to 27.997	3.286 to 27.999	2.919 to 27.878
Crystal size, mm	0.328x0.263x0.102	0.390x0.268x0.192	0.270x0.130x0.080
μ , mm ⁻¹	1.384	1.569	1.671
Reflections collected/ unique	27093 / 7681	27157 / 7716	8204 / 8204
R _{int}	0.0392	0.0376	0.0520
GOF on F ²	1.038	1.046	0.999
R ₁ , wR ₂ [I > 2 σ (I)]	0.0262, 0.0601	0.0237, 0.0469	0.0343, 0.0611
R ₁ , wR ₂ (all data)	0.0329, 0.0623	0.0312, 0.0484	0.0467, 0.0634
$\Delta\rho_{\text{max}}/\Delta\rho_{\text{min}}$, e/Å ³	0.894 / -1.096	0.454 / -0.553	0.926 / -0.609

Table S2. Selected bond lengths (Å) for the compounds **1-3**.

Bond	1	2	3
M(1)-O(1)	2.4500(15)	2.4074(13)	2.385(2)
M (1)-O(2)	2.5252(14)	2.4758(12)	2.459(2)
M (1)-O(3)	2.4918(15)	2.4564(14)	2.435(2)
M (1)-O(4)	2.5022(15)	2.4622(14)	2.449(2)
M (1)-O(5)	2.4628(15)	2.4249(13)	2.401(2)
M (1)-O(6)	2.5147(14)	2.4572(12)	2.455(2)
M (1)-O(7)	2.4878(17)	2.4546(16)	2.433(3)
M (1)-O(8)	2.4836(16)	2.4487(13)	2.425(2)
O(1)-C(1)	1.271(2)	1.271(2)	1.272(4)
O(2)-C(3')	1.259(3)	1.263(2)	1.264(4)
O(3)-C(8)	1.263(3)	1.262(2)	1.258(4)
O(4)-C(10')	1.262(3)	1.267(2)	1.261(4)
O(5)-C(15)	1.266(2)	1.266(2)	1.267(4)
O(6)-C(17')	1.265(2)	1.270(2)	1.268(4)
C(1)-C(2)	1.391(3)	1.391(3)	1.389(4)
C(1)-C(3')	1.552(3)	1.550(3)	1.560(4)
C(2)-C(3)	1.411(3)	1.409(2)	1.404(4)
C(8)-C(9)	1.403(3)	1.403(3)	1.403(5)
C(8)-C(10')	1.557(3)	1.553(2)	1.549(4)

C(9)-C(10)	1.404(3)	1.407(3)	1.407(5)
C(15)-C(16)	1.394(3)	1.405(3)	1.405(4)
C(15)-C(17')	1.552(3)	1.546(3)	1.543(4)
C(16)-C(17)	1.407(3)	1.401(2)	1.402(4)

Table S3. The parameters of porous structure of samples under investigation.

	Specific surface area / $\text{m}^2 \cdot \text{g}^{-1}$			$V_{\text{pore}} / \text{cm}^3 \cdot \text{g}^{-1}$		$V_{\text{ads}}(\text{CO}_2)^a / \text{cm}^3(\text{STP}) \cdot \text{g}^{-1}$
	Langmuir	BET	DFT	Total	DFT	
1	110.6	80.3	36.6	0.0445	0.0310	20.8
2	99.4	44.6	29.7	0.0532	0.0366	38.5
3	192.6	129.8	48.1	0.0645	0.0447	30.8

^a at $P/P_0 = 0.95$

Fig. S1. Pore size distribution curves for compounds **1** and **3**.

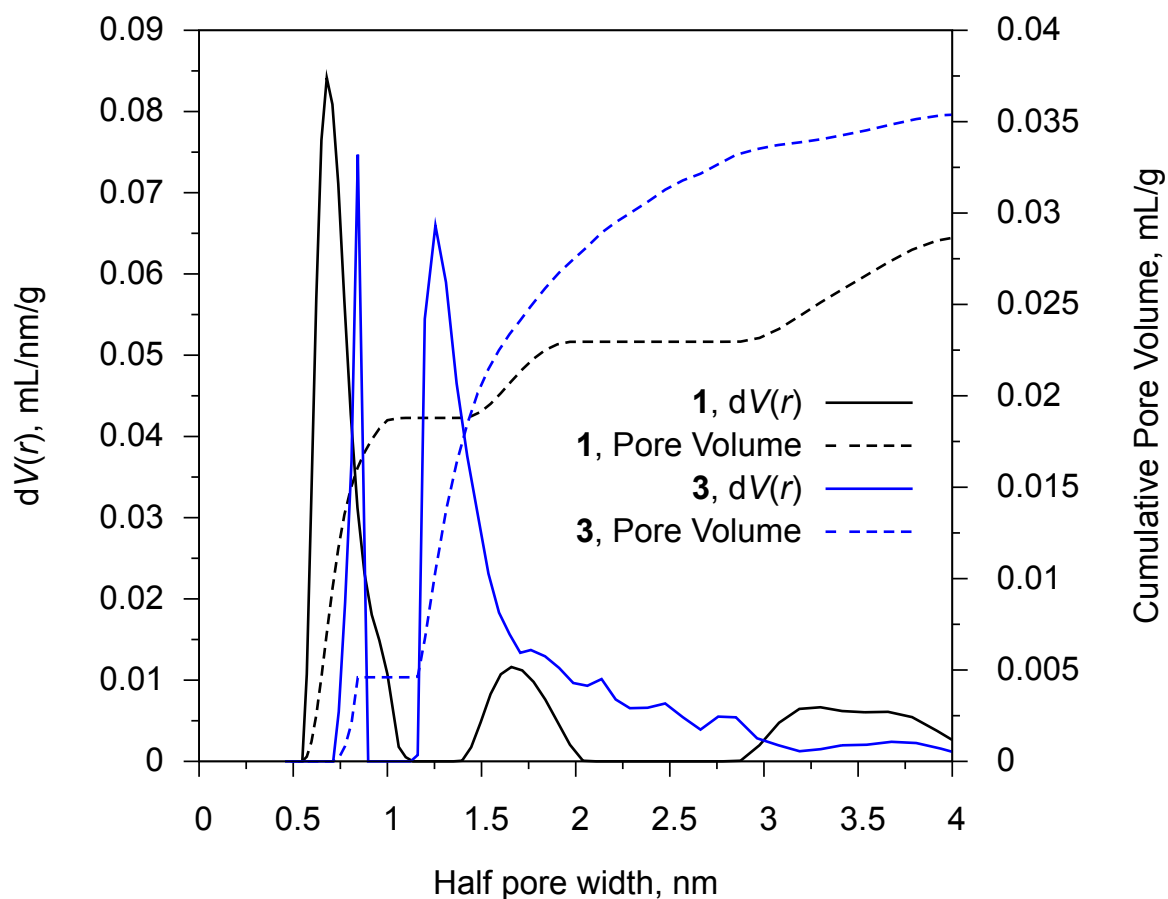


Fig. S2. CV of reduction for **1**. CPE, CH₃CN, 10⁻¹ M Bu₄NBF₄. Potentials vs. Ag/AgCl. Inset: Semi-Derivative of current vs potentials.

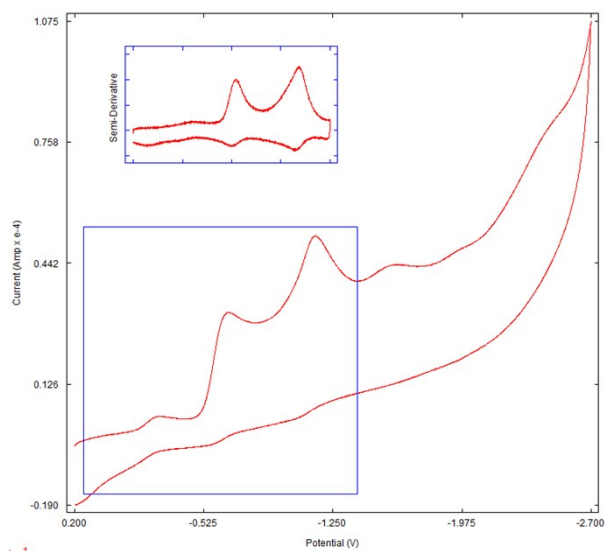


Fig. S3. CV of oxidation for **1**. CPE, CH₃CN, 10⁻¹ M Bu₄NBF₄. Potentials vs. Ag/AgCl. Inset: Semi-Derivative of current vs potentials.

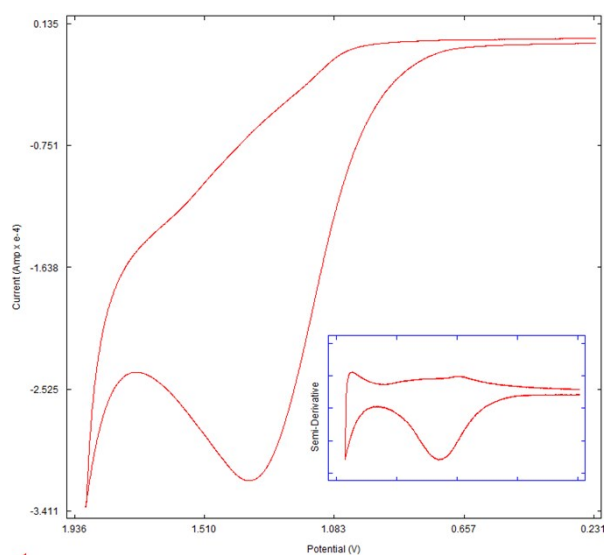


Fig. S4. CV of reduction for **2**. CPE, CH₃CN, 10⁻¹ M Bu₄NBF₄. Potentials vs. Ag/AgCl. Inset: Semi-Derivative of current vs potentials.

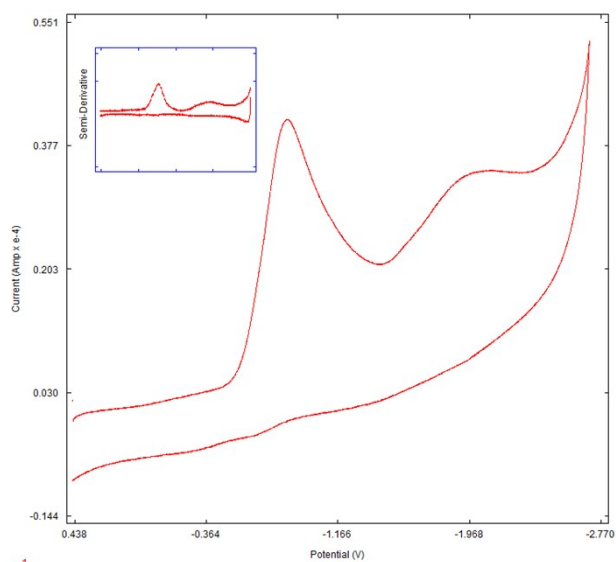


Fig. S5. CV of oxidation for **2**, CPE, CH₃CN, 10⁻¹ M Bu₄NBF₄. Potentials vs. Ag/AgCl. Inset: Semi-Derivative of current vs potentials.

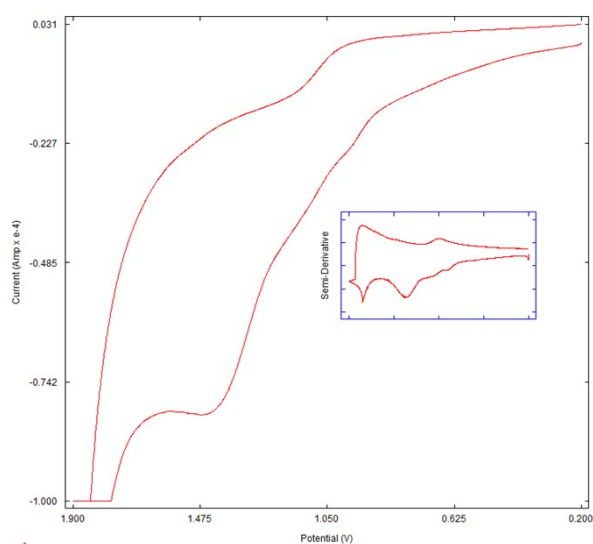


Fig. S6. CV of reduction for **3**. CPE, CH₃CN, 10⁻¹ M Bu₄NBF₄. Potentials vs. Ag/AgCl. Inset: Semi-Derivative of current vs potentials.

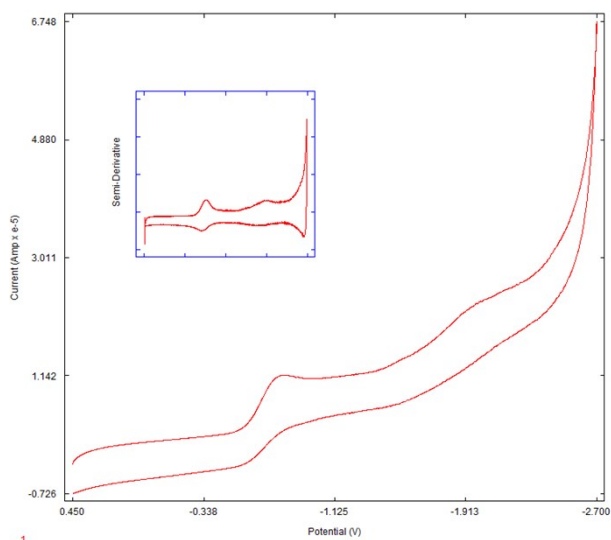


Fig. S7. CV of oxidation for **3**, CPE, CH₃CN, 10⁻¹ M Bu₄NBF₄. Potentials vs. Ag/AgCl. Inset: Semi-Derivative of current vs potentials.

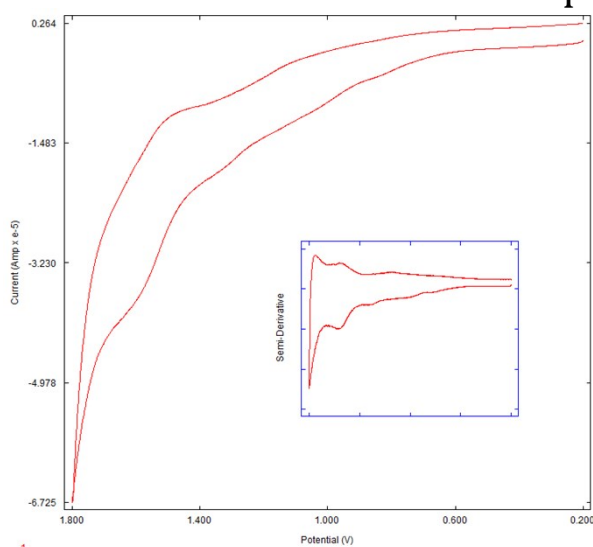


Table S4. Frontier orbitals energy levels.

Complex	E _{HOMO-1}	E _{LUMO-1}	ΔE _{HOMO-LUMO}
1	-5.58 eV	-3.74 eV	1.84 eV
2	-5.80 eV	-3.56 eV	2.24 eV
3	-5.90 eV	-3.62 eV	2.28 eV

$$(E_{\text{LUMO}} = -(E_{[\text{semidif,red vs. Fc}^+/\text{Fc}]} + 4.8), E_{\text{HOMO}} = (E_{[\text{semidif,red vs. Fc}^+/\text{Fc}]} + 4.8) [11]$$

Shape analysis.

 S H A P E v2.1 Continuous Shape Measures calculation

(c) 2013 Electronic Structure Group, Universitat de Barcelona

Contact: llunell@ub.edu

LnQuin

OP-8 1 D8h Octagon
 HPY-8 2 C7v Heptagonal pyramid
 HBPY-8 3 D6h Hexagonal bipyramid
 CU-8 4 Oh Cube
 SAPR-8 5 D4d Square antiprism
 TDD-8 6 D2d Triangular dodecahedron
 JGBF-8 7 D2d Johnson gyrobifastigium J26
 JETBPY-8 8 D3h Johnson elongated triangular bipyramid J14
 JBTPR-8 9 C2v Biaugmented trigonal prism J50
 BTPR-8 10 C2v Biaugmented trigonal prism
 JSD-8 11 D2d Snub diphenoid J84
 TT-8 12 Td Triakis tetrahedron

Structure [ML8]	OP-8	HPY-8	HBPY-8	CU-8	SAPR-8	TDD-8	JGBF-8	JETBPY-8	JBTPR-8	BTPR-8	JSD-8	TT-8	
LaQuin	,	31.969,	22.158,	14.803,	11.237,	2.605,	1.953,	12.131,	26.670,	2.772,	2.061,	3.839,	11.948
PrQuin	,	31.718,	22.356,	14.908,	11.024,	2.295,	1.849,	12.410,	27.060,	2.625,	1.895,	3.847,	11.734
NdQuin	,	31.496,	22.315,	15.019,	10.916,	2.127,	1.821,	12.485,	27.072,	2.566,	1.826,	3.794,	11.648

S H A P E v2.1 Continuous Shape Measures calculation

(c) 2013 Electronic Structure Group, Universitat de Barcelona

Contact: llunell@ub.edu

LnQuin

TDD-8 6 D2d Triangular dodecahedron

ocPB 0 C1 One-capped pentagonal bipyramid

Minimal distortion path analysis: from TDD-8 (0%) to ocPB (100%)

Deviation threshold to calculate Generalized Coordinate: 10.000%

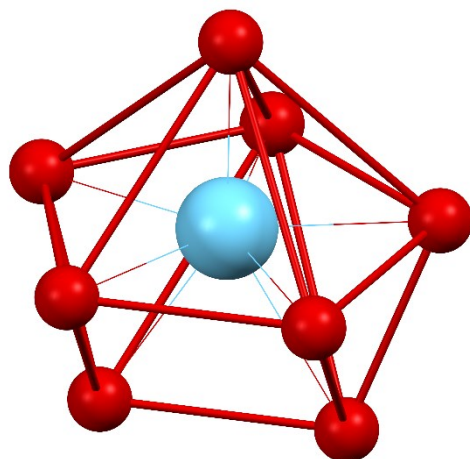
Structure [ML8]	TDD-8	ocPB	DevPath	GenCoord
------------------	-------	------	---------	----------

LaQuin	,	1.953,	1.612,	45.9,	-
--------	---	--------	--------	-------	---

PrQuin	,	1.849,	1.612,	43.8,	-
--------	---	--------	--------	-------	---

NdQuin	,	1.821,	1.692,	45.0,	-
--------	---	--------	--------	-------	---

Fig S8. User-defined perfect polyhedron – one-capped Pentagonal Bipyramid



Atom coordinates:

O	1.000000	0.000000	0.000000
O	0.309017	-0.951056	0.000000
O	-0.809017	-0.588785	0.000000
O	-0.809017	0.588785	0.000000
O	0.309017	0.951056	0.000000
O	0.000000	0.000000	1.000000
O	0.000000	0.588785	-1.000000
O	0.000000	-0.588785	-1.000000
Ln	0.000000	0.000000	0.000000

Fig. S9. PXRD patterns for **1** (blue line – experimental, red line – simulated).

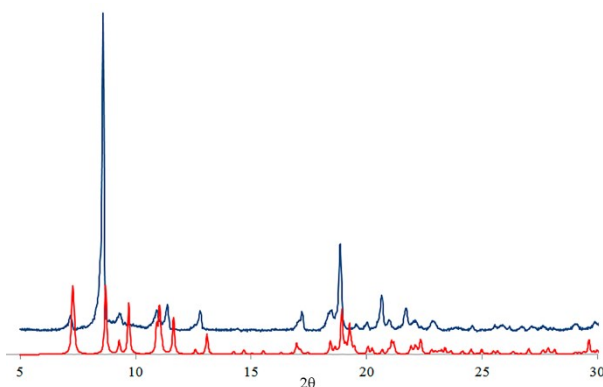


Fig. S10. PXRD patterns for **2** (blue line – experimental, red line – simulated).

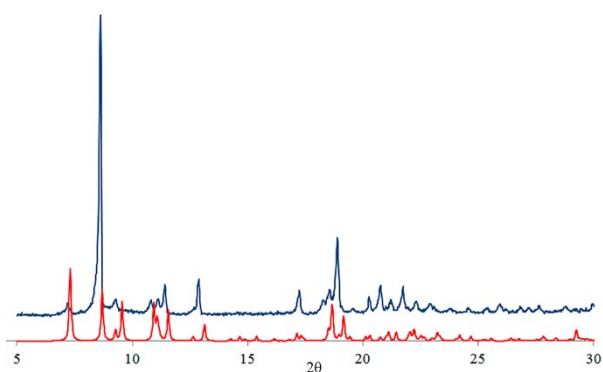
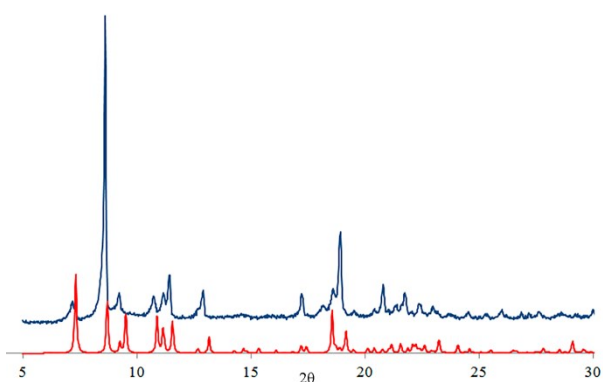


Fig. S11. PXRD patterns for **3** (blue line – experimental, red line – simulated).



References

- [1] N.M. Khamaletdinova, I.N. Meshcheryakova, A.V. Piskunov, O.V. Kuznetsova, *Journal of Structural Chemistry*, 2015, **56**, 233-242.
- [2] D.D. Perrin, W.L.F. Armarego, D.R. Perrin, *Purification of Laboratory Chemicals*, 1980. Oxford.
- [3] CrysAlis Pro - Software Package Agilent Technologies (2012)
- [4] Sheldrick GM (2000) SHELXTL V.6.12 Structure determination software suite Bruker AXS Madison.
- [5] R.C. Clark, J.S. Reid, *Acta Cryst. A*, 1995, **51**, 887-897
- [6] Thermophysical Properties of Fluid Systems, Database of National Institute of Standards and Technology, NIST. <http://webbook.nist.gov/chemistry/fluid/>
- [7] M.N. Khrizanforov, D.M. Arkhipova, R.P. Shekurov, T.P. Gerasimova, V.V. Ermolaev, D.R. Islamov, V.A. Miluykov, O.N. Kataeva, V.V. Khrizanforova, O.G. Sinyashin, Y.H. Budnikova, *J. Solid State Electrochem.*, 2015, **19**, 2883-2890.
- [8] O. Kataeva, M. Khrizanforov, Y. Budnikova, D. Islamov, T. Burganov, A. Vandyukov, K. Lyssenko, B. Mahns, M. Nohr, S. Hampel, M. Knupfer, *Cryst. Growth Des.*, 2016, **16**, 331-338.
- [9] M.N. Khrizanforov, S.V. Fedorenko, S.O. Strekalova, K.V. Kholin, A.R. Mustafina, M.Y. Zhilkin, V.V. Khrizanforova, Y.N. Osin, V.V. Salnikov, TV. Gryaznova, Y.H. Budnikova, *Dalton Transactions*, 2016, **45**, 11976-11982.
- [10] M.N. Khrizanforov, R.P. Shekurov, V.V. Ermolaev, D.M. Arkhipova, V.A. Miluykov, O.N. Kataeva, V.V. Khrizanforova, Y.H. Budnikova, *Phosphorus Sulfur Silicon Related Elements*, 2016, **191**, 1611-1612.
- [11] R.R. Zairov, A.V. Yagodin, M. Khrizanforov, A.G. Martynov, I.R. Nizameev, V. Syakaev, A. Gubaidullin, T. Kornev, O. Kaman, Y.H. Budnikova, Y.G. Gorbunova, A.R. Mustafina, *Journal of Nanoparticle Research*, 2019, **21**, 12.